Journal of Materials Chemistry A

PAPER

View Article Online
View Journal | View Issue

Cite this: J. Mater. Chem. A, 2016, 4, 3704

Preparation of flexible perovskite solar cells by a gas pump drying method on a plastic substrate†

Li-Li Gao,[a] Lu-Sheng Liang,[b] Xiao-Xuan Song,[a] Bin Ding,[a] Guan-Jun Yang,*[a] Bin Fan,[b] Cheng-Xin Li[a] and Chang-Jiu Li[a]

Received 9th January 2016
Accepted 20th January 2016

DOI: 10.1039/c6ta00230g

www.rsc.org/MaterialsA

A uniform and full coverage perovskite film is of significant importance for flexible perovskite solar cells. In this study, highly efficient flexible perovskite solar cells were assembled using a flexible conductive plastic substrate by a one-step gas pump drying method to prepare high performance perovskite films under air conditions. The SEM results show that the perovskite film deposited on the flexible conductive plastic substrate was uniform, compact, and pinhole-free. The AFM results show that the film presented an extremely smooth surface morphology with a root mean square roughness of 15.8 nm in a large and representative scan area of 18 × 18 μm^2. The flexible planar perovskite solar cell was fabricated, and all devices were prepared at 100 °C or below under air conditions. The highest efficiency on flexible substrates had reached 11.34% with an average efficiency of 8.93% for 14 solar cell devices.

Introduction

Organometal trihalide perovskite solar cells (PSCs) have attracted widespread academic and commercial interest due to a rapid increase in efficiency,[1–3] which has boosted from 3.8% (ref. 4) in 2009 to 20.1% (ref. 5) in 2014. These great achievements are mainly attributed to the unique characteristics of perovskite materials, such as low cost, high photo-to-electric conversion efficiency, high light absorption properties, direct bandgaps, high charge-carrier mobility and long electron–hole exciton transport distance (more than 1 μm).[6–8] Perovskite materials are soluble, which makes it quite easy and cheap to prepare perovskite solar cells.[9,10]

Plastic-based flexible solar cells have received extensive application and research attention due to their low-cost, light weight, portability and flexibility.[11–16] To utilize perovskite materials, the structure of flexible solar cells can be designed as a planar heterojunction, which can avoid the preparation of the mesoporous layer on a substrate surface.[2] It generally contains a flexible electrode, an electron transportation layer, a perovskite light absorption material, a hole transportation layer, and a counter electrode. The cell performance is influenced by many factors, among which the microstructure of perovskite films is crucial. When there are some pinholes in the perovskite film or even many bare substrate surfaces without perovskite covering, current shunting in the carrier transportation would inevitably occur, which degrades the device performance.[17,18] In addition, the light absorption ability of the film will be also reduced in the pinhole region and uncovered region. Therefore, a uniform and compact perovskite film is of crucial importance to achieve a solar cell of high efficiency.[19]

To date, solution processing is widely used in the preparation of perovskite films. It contains a one-step method and a two-step method.[20–22] In the two step method, it is difficult for lead iodide to react completely with iodine methylamine when lead iodide is dipped in iodine methylamine solvent, and the organometal trihalide film is rough.[21,22] Therefore, many attempts have been made to achieve a compact and pinhole-free film by the two-step method, such as changing soaking to dropping in the second step,[23] or the physical–chemical deposition process at ultra-low temperatures,[24] or alternating precursor layer deposition,[25] or the gas-assisted solution process,[26,27] or vapor deposition by the Snaith group.[10] The one-step method can avoid the problem related to the reaction between lead iodide and iodine methylamine, without any component heterogeneity. However, the processed film is often loosely packed with many pinholes, and dendritic grains usually present in the film, resulting in a partial coverage of the substrate.[21,22] Therefore, dropping anti-solvent in the spinning perovskite precursor solution,[28] or the PbAc-based method by Snaith,[29] or methylamine-gas induced defect-healing,[30] and solvent extraction method,[31] have been developed to improve the coverage of the film. All those approaches achieved progress in the preparation of perovskite films.

This paper aims at developing flexible perovskite solar cells with a compact and uniform perovskite film with a full coverage on a plastic substrate. For the solution processing method, reaching solution supersaturation is the necessary condition for

[a]State Key Laboratory for Mechanical Behavior of Materials, School of Materials Science and Engineering, Xi'an Jiaotong University, Xi'an, Shaanxi 710049, PR China. E-mail: ygj@mail.xjtu.edu.cn; licj@mail.xjtu.edu.cn

[b]Xiamen Weihua Solar Co. Ltd., Xiamen, 361100, PR China

† Electronic supplementary information (ESI) available. See DOI: 10.1039/c6ta00230g

crystallization. The higher the degree of supersaturation of the solute, the easier the precipitation of crystal nuclei.[32–35] In this paper, we reported that, when the gas phase pressure over the solution is lower than the saturated vapor pressure of the solvent at the current temperature, the solvent evaporates immediately. Based on this principle, we proposed a gas pump drying method for the liquid film in a low pressure, which is lower than the saturated vapor pressure of the solvent. The solvent evaporation can be significantly accelerated and, thereby, the liquid film reaches supersaturation rapidly, which results in rapid nucleation of the solute in the solution. In this study, perovskite $CH_3NH_3PbI_3$ films were prepared on a flexible ZnO coated ITO-PEN substrate by this novel gas pump drying process, and flexible planar perovskite solar cells were assembled. We achieved the highest power conversion efficiency (PEC) 11.34% with the average PEC of 8.93% $\pm$ 1.36%. The results indicate that the one-step gas pump drying process is an excellent method to prepare flexible solar cells. It is worth noting that this gas pump drying method can be operated just in air.

Experimental section

Materials and preparation

The materials used were lead iodide (PbI_2, 99.99%), *N*,*N*-dimethylformamide (DMF, 99.8%), iodine methylamine (CH_3NH_3I), and 2,2′,7,7′-tetrakis(*N*,*N*-di-*p*-methoxyphenylamine)-9,9-spirobifluorene (spiro-OMeTAD). Unless special instructions, all materials were purchased from Xiamen Weihua Solar Company, and used as received. Gas pump drying equipment used was home-designed by our group, as shown in Fig. 1.

Perovskite film deposition

ITO-PEN sheets (indium-doped tin oxide coated polyethylene terephthalate sheets, 15.6 Ω sq^{-1}) were rinsed successively with ethyl alcohol, deionized water in an ultrasonic bath for 10 min, and blow-dried by nitrogen. The flexible substrate was mounted onto a rigid glass substrate for easy device fabrication. ZnO, as the electron transportation layer, was prepared on the ITO-PEN substrate by magnetron sputtering at a pressure of 2 Pa using a ZnO target. The ZnO surface was treated with ozone and ultraviolet for 15 min. The perovskite precursor solution was composed of PbI_2 and CH_3NH_3I at a ratio of 1 : 1, which dissolved in DMF solvent at 70 °C. By dropping appropriate perovskite precursor solution on the ZnO-coated ITO-PEN surface and after spinning at a speed of 3000 rpm for 10 s, a faint yellow liquid perovskite precursor film about 2 μm was obtained. Fig. 1(a) illustrates the process of preparing perovskite films by the gas pump drying process. Fig. 1(b) schematically shows the gas pump drying system. Subsequently, moving the film quickly to a small sample chamber connected to the large low pressure chamber system, which had been pumped beforehand to below 10 Pa, the sample chamber was evacuated. After evacuating for *ca.* 40 s, a transparent brown perovskite film evolved. The film was annealed at 100 °C for 10 min, the brown film turned into a black film, and the film was still transparent.

Device fabrication and characterization

A 25 μL spiro-OMeTAD solution was spin-coated on perovskite films at 4000 rpm for 30 s. A 10 nm-thick MoO_3 and 150 nm-thick silver layer were deposited by thermal evaporation at a base pressure of 4×10^{-4} Pa. The completed devices were stored in a N_2-purged glovebox (<0.1 ppm O_2 and H_2O). Prior to the spinning of spiro-OMeTAD, all device fabrication steps were carried out under ambient conditions at a temperature of 23 °C and a humidity of 50%. All devices were prepared at 100 °C or below.

The surface of the prepared perovskite films was examined using a MIRA3 TESCAN scanning electron microscope (SEM).

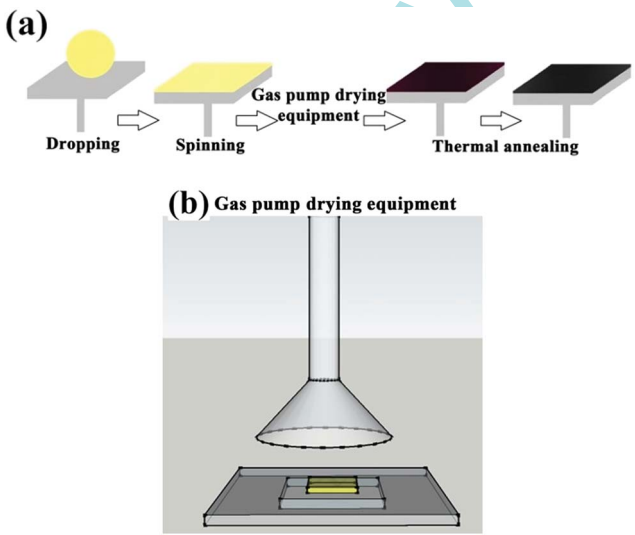

Fig. 1 Schematic procedure of preparing perovskite films by the one-step gas pump drying method (a) and the gas pump drying equipment (b).

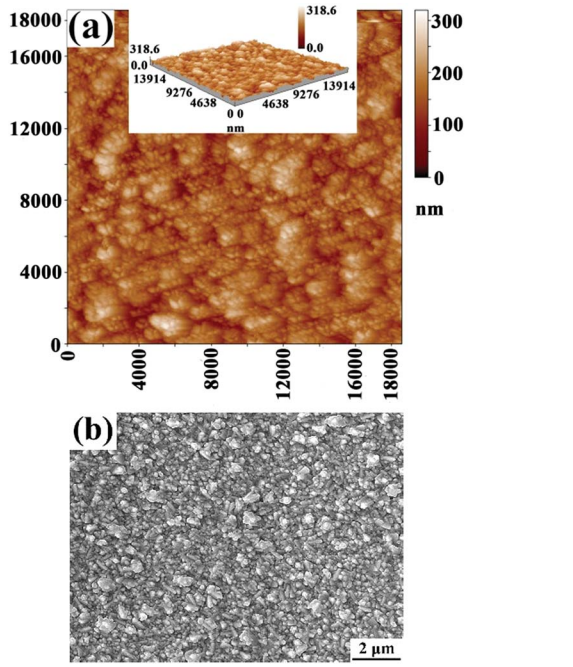

Fig. 2 Topography of the surface of ZnO-coated ITO-PEN (a) AFM (Inset: three-dimensional topographic image) and (b) SEM.

To examine the surface roughness, the film was characterized by BY2000 atomic force microscopy (AFM). The X-ray diffraction (XRD) patterns of the substrate and perovskite films were obtained with a D8 Advance X-ray diffractometer with Cu Kα radiation. The absorption spectra of the perovskite film were measured with a U-3010 spectrophotometer. Current–voltage (*I–V*) curves of the perovskite solar cells were measured by using a Keithley 2400 source-measure unit under an illumination of simulated sunlight, provided by a 450W Class AAA solar simulator equipped with an AM1.5G filter (Sol2A, Oriel Instruments). The exact light intensity was calibrated using a single-crystal silicon photovoltaic cell as the reference (91150V, Oriel Instruments); the light intensity was 86 mW cm^{-2}. The cells were fabricated with a metal mask covering an area of 0.09 cm^2 to receive sunlight.

Results and discussion

Microstructure of the perovskite film on a plastic substrate

Fig. 2 shows the surface morphology of ZnO-coated ITO-PEN, by both high resolution AFM and SEM. The substrate presents a rough surface morphology, which is a typical characteristic of sputtered films.[36,37] The root mean square (RMS) roughness of the deposited ZnO film is 28.60 nm. It is reported that a certain degree of roughness of the substrate surface is useful for the nucleation of perovskite.[33]

To demonstrate the structure of the perovskite film prepared on a flexible substrate by the gas pump drying method proposed in this study, we examined the perovskite film on the ZnO coated plastic ITO substrate by different methods, *i.e.* conventional heat drying and gas pump drying methods, using scanning electron microscopy. In the conventional scheme, the perovskite precursor solution is spin-coated at room temperature and then post-annealed for 10 min on a hot plate maintained at 100 °C. The film prepared by conventional spin-coating and drying is porous and the grains present a disorganized dendrite morphology (Fig. 3(a) and (b)). The film, made by the gas pump drying method, presents a smooth, compact and uniform morphology without any visible pinholes as shown in Fig. 3(c)–(f). Based on a statistical measurement of 626 grains, it was found that the grains having a size ranging from 200 to 600 nm account for 90%, as shown in Fig. 3(h), which indicates that the grain size distribution is quite uniform. Compared with conventional heat drying, the gas pump drying method enlarged the differential pressure between saturated vapor pressure and the pressure of the solvent at the liquid gas

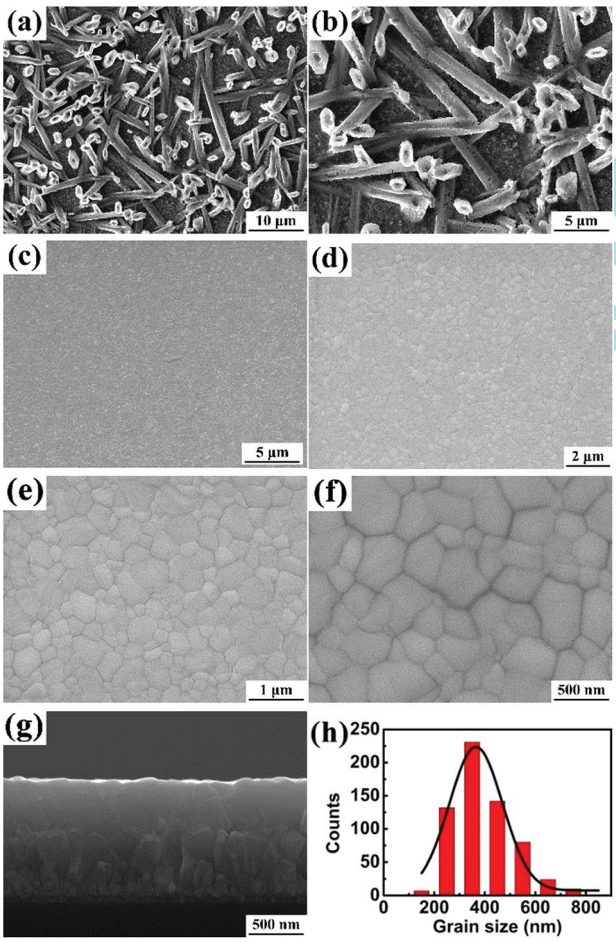

Fig. 3 SEM images of the perovskite film made by (a and b) conventional heat drying, (c–f) the gas pump drying method, (g) cross-section of the perovskite film made by the gas pump drying method, (h) grain size of perovskite distribution made by the gas pump drying method.

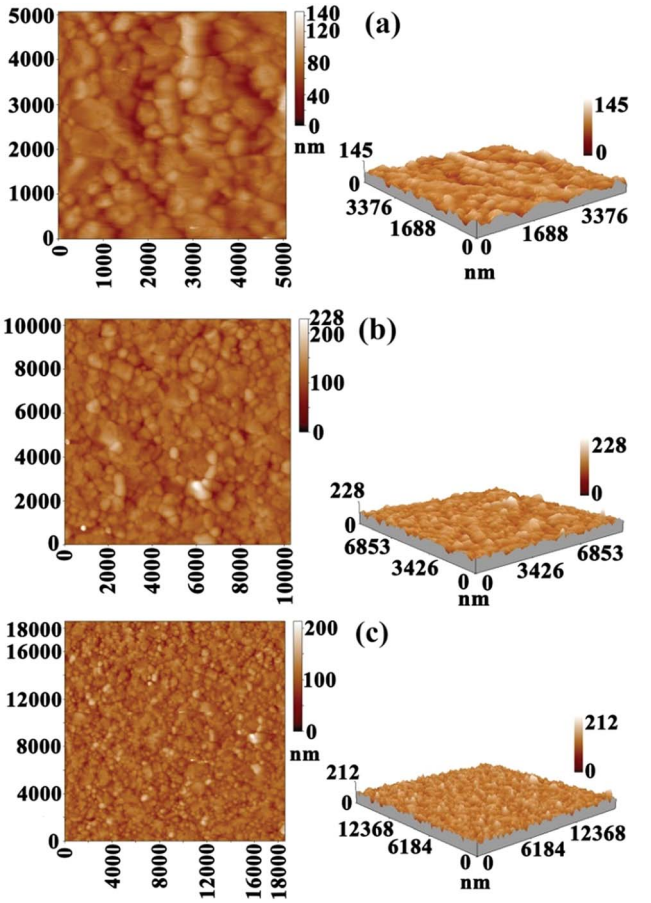

Fig. 4 AFM topographies of a perovskite film with a sweeping range of 5 × 5 μm^2 (a), 10 × 10 μm^2 (b), 18 × 18 μm^2 (c), respectively.

Table 1 Roughness comparison of perovskite films made by the one-step gas pump drying method and other reported methods

Method	Scanning area (μm^2)	Roughness average (R_a) (nm)	Root mean square (RMS) roughness (nm)
One-step gas pump drying method	18 × 18	12.3	15.8
	10 × 10	12.7	16.8
	5 × 5	9.96	12.7
Vapor-assisted[40]	5 × 5	23.2	—
Up-scalable approach[41]	5 × 5	27	—
Sequentially deposited[42]	5 × 5	21.2	—
Gas–solid crystallization[27]	3 × 3	26.3	32.8
Alternating precursor layer deposition[25]	10 × 10	—	26.8
Vacuum-assisted thermal annealing[38]	5 × 5	—	9.59
Solvent engineering process[28]	3 × 3	—	8.3
Successive spin-coating/annealing[39]	2 × 2	—	12

interface, which would accelerate solvent evaporation. In this way, the solvent reaches a very high degree of supersaturation in a short time, and large numbers of heterogeneous nuclei form on the substrate and grow into columnar crystals. The clear close-packed columnar crystals are shown in Fig. 3(g). The gas pump drying method can be used to dry not only perovskite films, but also lead iodide films.

To quantitatively investigate the smooth perovskite film surface profile, we measured the surface roughness of the perovskite films made by conventional heat and gas pump drying with high resolution AFM. The measurements were made in three different scanning areas, *i.e.* 5 × 5 μm^2, 10 × 10 μm^2 and 18 × 18 μm^2. To make the results statistically informative, we chose the scanning area randomly from a large and uniform perovskite film with a size of 0.09 cm^2, which is the solar cell area. Fig. 4(a)–(c) show the AFM images of perovskite films made by gas pump drying and the corresponding three-dimensional morphologies. It demonstrates a quite uniform surface profile despite very different scanning sizes. The RMS was 12.7 nm, 16.8 nm and 15.8 nm, respectively, in 5 × 5 μm^2, 10 × 10 μm^2 and 18 × 18 μm^2 scanning areas. The AFM image of the perovskite film made by conventional heat drying is shown in Fig. S1,† and the RMS is 77.4 nm in a 10 × 10 μm^2 scanning area. In order to further comprehensively compare the surface roughness, we collected very detailed information from the reported literature. Table 1 shows the roughness of perovskite films made by the one-step gas pump drying method and other methods reported for comparison. Very small RMS roughness can be found as 9.59 nm, 8.3 nm, and 12 nm, while the scanning area is as small as 5 × 5 μm^2, 3 × 3 μm^2, and 2 × 2 μm^2.[28,38,39] Comparing the above mentioned three groups of data, one can find that the RMS increases with increasing scanning area. However, if the scanning area is larger than 10 × 10 μm^2, the result of RMS tends to be a stable and representative value. Therefore, it can be concluded that an effective and representative measurement of RMS for perovskite films should reach, at least, an area of 10 × 10 μm^2. The perovskite film RMS, prepared by the gas pump drying method, was 16.8 nm (for a scanning area of 10 × 10 μm^2), which was much lower than the obtained value in the reported literature at such an effective scanning area.[25]

For a high-efficiency cell, the perovskite film must cover the substrate without a pin-hole in the whole area. Considering the extremely small RMS of the perovskite film in this study, the perovskite film is a homogeneous film without a large area of uncovered substrate surface, which can also be proved by the film surface morphology shown in Fig. 3. However, to make sure that there is no pinhole in the film, we have to carefully compare the maximum surface fluctuation (especially the maximum concave depth) with the film thickness. From the three-dimensional image in Fig. 4, faint surface fluctuations can be easily found. The quantitative results show that the maximum

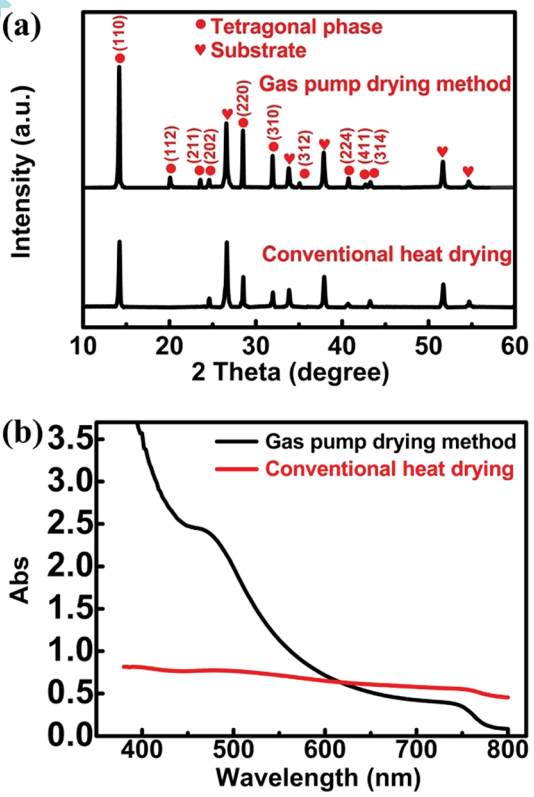

Fig. 5 XRD patterns of the perovskite film made by conventional heat drying and gas pump drying (substrate diffraction peak have been marked) (a), UV-visible absorption spectrum of perovskite films made by the gas pump drying method and conventional heat drying (b).

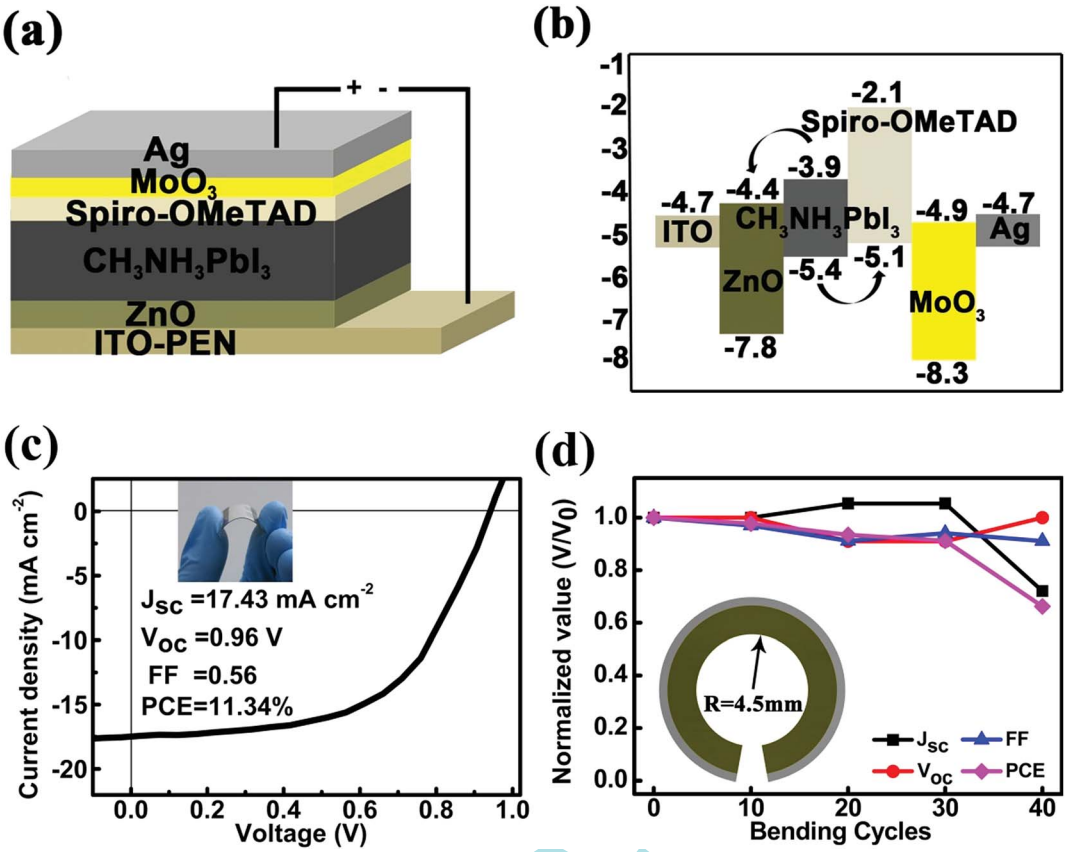

Fig. 6 Schematic structure of a perovskite solar cell (a), and energy level alignment of various device layers (b). The current–voltage curve of the highest efficiency cell from short-circuit to forward bias (SC-FB) (c), inset is a photographic representation of the flexible device. Normalized value as a function of number of bending cycles (d), inset is a bending diagram.

of the concave is 60 nm, 80 nm and 70 nm for the scanning area of 5 × 5 μm^2, 10 × 10 μm^2 and 18 × 18 μm^2, respectively. The largest value of the maximum concave depth, 70 nm for a large scanning area of 18 × 18 μm^2, is still much smaller than the average film thickness, *ca.* 500 nm in this study. Therefore, it can be concluded that the perovskite film on the flexible substrate in this study is of a pinhole-free structure.

Crystallization and absorption of perovskite films

Fig. 5(a) shows the XRD patterns of perovskite films made by conventional heat drying and gas pump drying methods. Both of them show strong diffraction peaks at the 2θ of 14.1°, 28.4° and 31.8°, which corresponds to the tetragonal phase of (110), (220) and (310) crystal planes. However, there were some inferior diffraction peaks in the perovskite film made by gas pump drying, (112), (211), (312) and (224) at the 2θ of 20.2°, 23.6°, 35.1° and 40.8°. They all clearly showed the existence of the tetragonal phase (space group *I*4/*mcm*, $a = b = 8.8743$ Å, and $c = 12.6708$ Å) in the film.[43]

To further evaluate the optical property of the perovskite film prepared on the flexible substrate, we measured the UV-visible absorption spectra of perovskite films, which were made by gas pump drying and conventional heat drying, as shown in Fig. 5(b). The perovskite film made by the gas pump drying method presents a very high absorption intensity from 380 m to 620 nm than the film made by conventional drying. Because of the huge scattering effect by dendrite crystals, the perovskite film made by conventional heat drying presents a higher absorption from 620 nm to 800 nm. The absorption of the perovskite film made by gas pump drying extends over the complete visible spectrum up to 760 nm, with a local maximum around 500 nm, which is consistent with the results reported.[44–46]

Photovoltaic performance of flexible perovskite solar cells

To examine the photovoltaic performance of the flexible solar cells with perovskite films on the plastic substrate surface, we assembled planar solar cells as shown in Fig. 6. Fig. 6(a) shows the schematic structure of a flexible plane perovskite solar cell, and Fig. 6(b) shows its corresponding energy level of every layer. For an efficient blocking layer, a compact film is necessary and critical to prevent the contact between the hole transport layer and ITO layers. The ZnO film, made by magnetron sputtering, can be compact enough to stop charge transport across the film. Compared to the TiO_2 compact layer, ZnO is also a viable alternative due to its comparable energy level as well as good electron transport properties.[47] ZnO has the energy level of −4.4 eV, which is a good match with the perovskite layer of −3.9 eV. Prior to the

$CH_3NH_3PbI_3$ solution loading, the ZnO surface was treated with ozone and ultraviolet to increase surface wettability.

To guarantee the reproducibility of the results, we prepared 14 devices and tested all of them. The statistical results of the photovoltaic performance of 14 devices yielded an average short-circuit photocurrent, J_{sc}, of 16.02 ± 1.53 mA cm^{-2}, open-circuit photovoltage, V_{oc}, of 0.94 ± 0.06 V, fill factor, and FF, of 0.5 ± 0.05, and thereby power-conversion efficiency, PCE, of 8.93 ± 1.36% (Table S1†). Among the 14 devices, we achieved the highest efficiency of 11.34%. Fig. 6(c) shows the current–voltage curve of the champion cell of the best PCE, presenting the J_{sc} of 17.43 mA cm^{-2}, V_{oc} of 0.96 V, and FF of 0.56. Another 14 flexible devices were prepared by the conventional heat drying method. Those devices yielded poor performance with an average J_{sc} of 0.67 ± 0.09 mA cm^{-2}, V_{oc} of 0.69 ± 0.08 V, FF of 0.52 ± 0.04, and PCE only of 0.29 ± 0.04%. The bad photovoltaic performance mainly could be attributed to the cell shunting and poor light absorption arising from the incomplete surface coverage. The detailed photovoltaic parameters are shown in Fig. S2.† The results of those flexible devices proved the reproducibility of flexible plane perovskite solar cells made by the one-step gas pump drying method.

In order to investigate the flexibility of the flexible PSC, preliminary bending tests were conducted on flexible planar PSC devices on the polymer substrate. We bent them to a small radius of just 4.5 mm, which is one of the highest bending extent (the smallest radius) compared with reports,[15,16,48–50] up to 40 cycles. The stability of the flexible PSC is shown in Fig. 6(d). The thickness of all device layers is *ca.* 1.3 μm, while the ITO-PEN substrate is *ca.* 200 μm. So a stress neutral layer exists in the flexible substrate when the flexible device is bent. Extremely small degradation of the efficiency of the flexible PSC was found within 30 bending cycles. This suggested a quite good flexibility of the flexible PSC. After the further 10 bending cycles, the devices exhibited 67% of initial efficiency. The decrease of efficiency during severe bending may be attributed to the degradation of the device layers.

Conclusion

In summary, using a one-step gas pump drying method at room temperature under air conditions, we prepared flexible perovskite solar cells with a uniform and full coverage compact perovskite film on a flexible conductive plastic substrate. The perovskite film presented an extremely smooth surface morphology. The RMS increased with increasing scanning area and tended to a stable and representative value when the scanning area was larger than 10 × 10 μm^2. The RMS of the perovskite film on the flexible substrate prepared in this study was *ca.* 16 nm in a large scan area of >10 × 10 μm^2. The perovskite grains presented a close-packed columnar structure with a uniform grain size, thereby forming a full coverage on the substrate surface. The best efficiency of the flexible planar perovskite solar cell has reached 11.34% with an average efficiency of 8.93% for 14 flexible solar cell devices. This method offers great promise for solar cells towards high efficiency flexible perovskite solar cells.

Acknowledgements

This work was supported by the National Program for Support of Top-notch Young Professionals.

References

1 N. G. Park, *Mater. Today*, 2015, **18**, 65–72.
2 H. S. Kim, S. H. Im and N. G. Park, *J. Phys. Chem. C*, 2014, **118**, 5615–5625.
3 G. Hodes, *Science*, 2013, **342**, 317–318.
4 A. Kojima, K. Teshima, Y. Shirai and T. Miyasaka, *J. Am. Chem. Soc.*, 2009, **131**, 6050.
5 W. S. Yang, J. H. Noh, N. J. Jeon, Y. C. Kim, S. Ryu, J. Seo and S. I. Seok, *Science*, 2015, **348**, 1234–1237.
6 S. Bai, Z. W. Wu, X. J. Wu, Y. Z. Jin, N. Zhao, Z. H. Chen, Q. Q. Mei, X. Z. Wang, Z. Ye, T. Y. Song, R. Y. Liu, S. T. Lee and B. Q. Sun, *Nano Res.*, 2014, **7**, 1749–1758.
7 Q. F. Dong, Y. J. Fang, Y. C. Shao, P. Mulligan, J. Qiu, L. Cao and J. S. Huang, *Science*, 2015, **347**, 967–970.
8 S. D. Stranks, G. E. Eperon, G. Grancini, C. Menelaou, M. J. P. Alcocer, T. Leijtens, L. M. Herz, A. Petrozza and H. J. Snaith, *Science*, 2013, **342**, 341–344.
9 M. M. Lee, J. Teuscher, T. Miyasaka, T. N. Murakami and H. J. Snaith, *Science*, 2012, **338**, 643–647.
10 M. Z. Liu, M. B. Johnston and H. J. Snaith, *Nature*, 2013, **501**, 395.
11 S. S. Shin, W. S. Yang, J. H. Noh, J. H. Suk, N. J. Jeon, J. H. Park, J. S. Kim, W. M. Seong and S. Il Seok, *Nat. Commun.*, 2015, **6**, 7410.
12 T. Liu, L. J. Zuo, T. Ye, J. K. Wu, G. B. A. Xue, W. F. Fu and H. Z. Chen, *RSC Adv.*, 2015, **5**, 94752–94758.
13 D. Yang, R. X. Yang, J. Zhang, Z. Yang, S. Z. Liu and C. Li, *Energy Environ. Sci.*, 2015, **8**, 3208–3214.
14 W. M. Qiu, U. W. Paetzold, R. Gehlhaar, V. Smirnov, H. G. Boyen, J. G. Tait, B. Conings, W. M. Zhang, C. B. Nielsen, I. McCulloch, L. Froyen, P. Heremans and D. Cheyns, *J. Mater. Chem. A*, 2015, **3**, 22824–22829.
15 M. M. Tavakoli, K. H. Tsui, Q. P. Zhang, J. He, Y. Yao, D. D. Li and Z. Y. Fan, *ACS Nano*, 2015, **9**, 10287–10295.
16 M. Lee, Y. Jo, D. S. Kim, H. Y. Jeong and Y. Jun, *J. Mater. Chem. A*, 2015, **3**, 14592–14597.
17 T. Salim, S. Y. Sun, Y. Abe, A. Krishna, A. C. Grimsdale and Y. M. Lam, *J. Mater. Chem. A*, 2015, **3**, 8943–8969.
18 L. Cojocaru, S. Uchida, A. K. Jena, T. Miyasaka, J. Nakazaki, T. Kubo and H. Segawa, *Chem. Lett.*, 2015, **44**, 1089–1091.
19 T. B. Song, Q. Chen, H. P. Zhou, C. Y. Jiang, H. H. Wang, Y. Yang, Y. S. Liu, J. B. You and Y. Yang, *J. Mater. Chem. A*, 2015, **3**, 9032–9050.
20 J. Burschka, N. Pellet, S. J. Moon, R. Humphry-Baker, P. Gao, M. K. Nazeeruddin and M. Gratzel, *Nature*, 2013, **499**, 316.
21 J. H. Im, H. S. Kim and N. G. Park, *APL Mater.*, 2014, **2**, 081510.
22 B. E. Cohen, S. Gamliel and L. Etgara, *APL Mater.*, 2014, **2**, 081502.
23 J. H. Im, I. H. Jang, N. Pellet, M. Gratzel and N. G. Park, *Nat. Nanotechnol.*, 2014, **9**, 927–932.

24 Y. K. Peng, G. S. Jing and T. H. Cui, *J. Mater. Chem. A*, 2015, **3**, 12436–12442.
25 D. Yang, Z. Yang, W. Qin, Y. L. Zhang, S. Z. Liu and C. Li, *J. Mater. Chem. A*, 2015, **3**, 9401–9405.
26 Z. G. Xiao, C. Bi, Y. C. Shao, Q. F. Dong, Q. Wang, Y. B. Yuan, C. G. Wang, Y. L. Gao and J. S. Huang, *Energy Environ. Sci.*, 2014, **7**, 2619–2623.
27 F. Hao, C. C. Stoumpos, Z. Liu, R. P. H. Chang and M. G. Kanatzidis, *J. Am. Chem. Soc.*, 2014, **136**, 16411–16419.
28 N. J. Jeon, J. H. Noh, Y. C. Kim, W. S. Yang, S. Ryu and S. Il Seol, *Nat. Mater.*, 2014, **13**, 897–903.
29 W. Zhang, M. Saliba, D. T. Moore, S. K. Pathak, M. T. Horantner, T. Stergiopoulos, S. D. Stranks, G. E. Eperon, J. A. Alexander-Webber, A. Abate, A. Sadhanala, S. H. Yao, Y. L. Chen, R. H. Friend, L. A. Estroff, U. Wiesner and H. J. Snaith, *Nat. Commun.*, 2015, **6**, 6142.
30 Z. M. Zhou, Z. W. Wang, Y. Y. Zhou, S. P. Pang, D. Wang, H. X. Xu, Z. H. Liu, N. P. Padture and G. L. Cui, *Angew. Chem., Int. Ed.*, 2015, **54**, 9705–9709.
31 Y. Zhou, M. Yang, W. Wu, A. L. Vasiliev, K. Zhu and N. P. Padture, *J. Mater. Chem. A*, 2015, **3**, 8178–8184.
32 M. Mukhopadhyay and S. V. Dalvi, *J. Chem. Technol. Biotechnol.*, 2005, **80**, 445–454.
33 C. V. Thompson, *Annu. Rev. Mater. Sci.*, 2000, **30**, 159–190.
34 A. Cacciuto, S. Auer and D. Frenkel, *Nature*, 2004, **428**, 404–406.
35 D. W. Oxtoby, *Acc. Chem. Res.*, 1998, **31**, 91–97.
36 H. Belaid, M. Nouiri, Z. Ben Ayadi, K. Djessas and L. El Mir, *J. Mater. Sci.: Mater. Electron.*, 2015, **26**, 8272–8276.
37 L. X. Chen, S. Liu, C. M. Li, Y. C. Wang, J. L. Liu and J. J. Wei, *Int. J. Miner., Metall. Mater.*, 2015, **22**, 1108–1114.
38 F. X. Xie, D. Zhang, H. M. Su, X. G. Ren, K. S. Wong, M. Gratzel and W. C. H. Choy, *ACS Nano*, 2015, **9**, 639–646.
39 Y. Kutes, L. H. Ye, Y. Y. Zhou, S. P. Pang, B. D. Huey and N. P. Padture, *J. Phys. Chem. Lett.*, 2014, **5**, 3335–3339.
40 Q. Chen, H. P. Zhou, Z. R. Hong, S. Luo, H. S. Duan, H. H. Wang, Y. S. Liu, G. Li and Y. Yang, *J. Am. Chem. Soc.*, 2014, **136**, 622–625.
41 Z. Yang, B. Cai, B. Zhou, T. T. Yao, W. Yu, S. Z. Liu, W. H. Zhang and C. Li, *Nano Energy*, 2015, **15**, 670–678.
42 L. Hu, J. Peng, W. W. Wang, Z. Xia, J. Y. Yuan, J. L. Lu, X. D. Huang, W. L. Ma, H. B. Song, W. Chen, Y. B. Cheng and J. Tang, *ACS Photonics*, 2014, **1**, 547–553.
43 T. Baikie, Y. N. Fang, J. M. Kadro, M. Schreyer, F. X. Wei, S. G. Mhaisalkar, M. Graetzel and T. J. White, *J. Mater. Chem. A*, 2013, **1**, 5628–5641.
44 Y. F. Chiang, J. Y. Jeng, M. H. Lee, S. R. Peng, P. Chen, T. F. Guo, T. C. Wen, Y. J. Hsu and C. M. Hsu, *Phys. Chem. Chem. Phys.*, 2014, **16**, 6033–6040.
45 O. Malinkiewicz, A. Yella, Y. H. Lee, G. M. Espallargas, M. Graetzel, M. K. Nazeeruddin and H. J. Bolink, *Nat. Photonics*, 2014, **8**, 128–132.
46 S. A. Kulkarni, T. Baikie, P. P. Boix, N. Yantara, N. Mathews and S. Mhaisalkar, *J. Mater. Chem. A*, 2014, **2**, 9221–9225.
47 J. X. Song, J. Bian, E. Q. Zheng, X. F. Wang, W. J. Tian and T. Miyasaka, *Chem. Lett.*, 2015, **44**, 610–612.
48 B. J. Kim, D. H. Kim, Y. Y. Lee, H. W. Shin, G. S. Han, J. S. Hong, K. Mahmood, T. K. Ahn, Y. C. Joo, K. S. Hong, N. G. Park, S. Lee and H. S. Jung, *Energy Environ. Sci.*, 2015, **8**, 916–921.
49 M. Lee, Y. Jo, D. S. Kim and Y. Jun, *J. Mater. Chem. A*, 2015, **3**, 4129–4133.
50 M. Dianetti, F. Di Giacomo, G. Polino, C. Ciceroni, A. Liscio, A. D'Epifanio, S. Licoccia, T. M. Brown, A. Di Carlo and F. Brunetti, *Sol. Energy Mater. Sol. Cells*, 2015, **140**, 150–157.